UNIZIK JOURNAL OF ENGINEERING AND APPLIED SCIENCES (UJEAS)

Research Article

Investigating the corrosion inhibition potentials of a pyrrolidinium-based ionic liquid on aluminium in acidic medium

Nkuzinna O.C., Onukwuili O.D

Special Issue
A Themed Issue in Honour of Professor Ekedimogu Eugene Nnuka on His retirement.

This themed issue honors Professor Ekedimogu Eugene Nnuka, celebrating his distinguished career upon his retirement. His legacy of exemplary scholarship, mentorship, and commitment to advancing knowledge is commemorated in this collection of works.

Edited by
Chinonso Hubert Achebe PhD.
Christian Emeka Okafor PhD.

UJEAS

UNIZIK JOURNAL OF ENGINEERING AND APPLIED SCIENCES

UNIZIK Journal of Engineering and Applied Sciences 3(2), June (2024), 718-734
Journal homepage: https://journals.unizik.edu.ng/index.php/ujeas
PRINT ISSN: 2992-4383 || ONLINE ISSN: 2992-4391

Investigating the corrosion inhibition potentials of a pyrrolidinium-based ionic liquid on aluminium in acidic medium

Nkuzinna O.C.[1*], Onukwuili O.D.[2]
[1]Department of Chemical Engineering, School of Engineering and Engineering Technology, Federal University of Technology, Owerri, P.M.B.1526,Imo State, Nigeria
[2]Department of Chemical Engineering, Nnamdi Azikiwe University, P. M. B. 5025, Awka, Nigeria *Corresponding author, Email address: nkuzinnachris@gmail.com

Abstract
The green ionic liquid 1-butyl-1-methylpyrrolidinium bromide [BMPyr]Br has been investigated for its anti-corrosion properties for aluminium in 1MHCl utilizing weight loss, electrochemical and computational techniques. The molecular structure of the obtained [BMPyr]Br was verified and characterized by FTIR spectroscopy. The Langmuir adsorption isotherm accurately described the adsorption behavior of the inhibitor. The corrosion test results from weight loss (WL), electrochemical impedance spectroscopy (EIS) and potentiodynamic polarization (PDP) reveal an impressive corrosion inhibition performance with efficiencies of 91.75%, 80.2% and 89.99% respectively with 45x 10^{-4}M at 313K. The PDP curve suggests that [BMPyr]Br operated as a mixed-type inhibitor. The experimental and theoretical findings (from DFT and MD) are in perfect accord, providing robust evidence that [BMPyr]Br is a highly effective corrosion inhibitor, with all approaches converging to a consistent conclusion.

Keywords: Ionic liquid, Corrosion inhibition, Aluminum, Weight loss, EIS, DFT.

1. Introduction

Aluminium is the second most commonly used metal due to its fascinating properties, including low atomic mass, light weight, good thermal and electrical conductivity, and low standard electrode potential (Verma *et al*., 2017). Aluminum's ability to resist corrosion in aqueous conditions is attributed to the swift development of a tightly packed, firmly adhering, and unbroken oxide coating. As a result, aluminum and its alloys have potential applications in areas such as of aircraft, marine, kitchen, military, vehicle, and the production of reaction vessels, pipelines, equipment, and chemical batteries (Ortega *et al*., 2021; El-Saeed *et al*., 2022). While the oxide layer formed on aluminium surface provides protection in certain circumstances, it can be worn away and the metal can corrode when exposed specific acidic and alkaline substances especially those containing chlorides (Xhanari and Finsgar, 2019). The negative repercussions of corrosion can be significantly reduced by adopting highly corrosion-resistant materials, design upgrades, protective coatings, electrochemical processes (cathodic and anodic protection), and the introduction of inhibitors (Byrne and Norton, 2016; Tang *et al*., 2017; Trabanelli, 2020). Corrosion inhibitors have an advantage over other approaches since they are more cost-effective, practicable, reliable and simple to use (Likhanova *et al*., 2019; Cao *et al*., 2020).

Corrosion inhibitors come in a variety of forms, such as nano-composites, synthetic organic compounds, surfactants, polymers and drugs (such as antifungals) which are frequently employed to prevent metal from corroding when exposed to acidic liquids (Deyab *et al*., 2017; Nkuna *et al*., 2020). Localized corrosion is generally prevented by the action of adsorptive inhibitors that prevent the aggressive anions from adsorbing to the metal surface, or by the creation of a more resistant oxide coating on the metal surface (Zhang *et al*., 2020). Recent advancements in the field of corrosion science and engineering have been devoted towards the design, development, and application of environmentally acceptable alternatives to traditional harmful corrosion inhibitors in the light of growing ecological

consciousness (Verma *et al*., 2020). Because of their natural and/or biological origins and non-toxic character, scientists have recently attempted to produce plant extracts and drugs as green corrosion inhibitors. However, extracting and purifying plant extracts are time-consuming, labour intensive, expensive, and necessitates a huge volume of organic solvents (Verma *et al*., 2018). Ionic liquids (ILs) have emerged as a promising green and long-term corrosion inhibitor among a variety of corrosion inhibitors (Deyab, 2020). Ionic liquids are molecules that consist of anions and cations that have an organic molecular structure that prevents efficient tight packing and have a unique combination of physical and chemical properties (Kabzar and Fatyeyeva, 2021). Ionic liquids are excellent sustainable alternatives to conventional corrosion inhibitors because they are associated with several environmentally friendly properties such as low toxicity, low melting point, high polarity, low vapour pressure, and high resistivity to thermal and chemical treatment (Atta *et al*., 2016; Yesudass *et al*., 2016; Cao *et al*., 2019; Dermani *et al*., 2019; Su *et al*., 2020; Quraishi, 2021).

There are several conceivable blends of cations and counter-anions in ionic liquids; pyrrolidinium based ILs have been widely reported and explored. Previous research has demonstrated that various ionic liquids based on the pyrrolidinium group exhibit strong corrosion prevention characteristics against numerous metals (El-Shamy *et al*., 2015; El- Katori and Abousalem, 2019; Abass *et al*., 2021; Zunita and Kevin, 2022). However, pyrrolidinium-based ionic liquids containing halide anions as corrosion inhibitors, particularly on aluminium, have not been well investigated. The current study was designed with the requirement for an efficient and cost-effective corrosion management technique in mind, as well as the go-green concept. In this study, the corrosion control ability of newly synthesized 1-butyl-1-methylpyrrolidinium bromide was investigated for aluminium corrosion in 1.0 M HCl. This work employed weight loss, potentiodynamic polarization (PDP), electrochemical impedance spectroscopy (EIS), structural characterization, surface examination and computational studies to evaluate the inhibitive capability of 1-butyl- 1-methylpyrrolidium bromide on aluminium induced in 1.0 M HCl solution.

2.0 Material and methods

2.1 Sourcing and preparation of Metal

The composition of the aluminium coupon utilized in the investigation is as follows: Fe(0.02%), Si(0.25%), Zn(0.07%), Mn(0.14%), Mg(0.03%), V(0.04%), Ti(0.12%), Cu(0,03%) and Al(99.3%). The coupons were cut to 3 x 3 x 0.2cm, polished with various grades of emery paper (600 to 1200), degreased with acetone, completely rinsed with distilled water, dried with heated air, and stored in a tight container for future use.

2.2. Synthesis of ionic Liquid

9.0g 0f n-bromobutane was added slowly to distilled methylpyrrolidine (5g) in a 250ml flat bottom flask fitted with a reflux condenser. The addition was at the rate that temperature of the solution did not get above 40^0C. The mixture was microwaved with microwave oven at 80% power level for 4minutes. The mixture was stirred with a magnetic stirrer for 1hour at 70^0C. It was cooled at room temperature. The liquid was decanted away from the yellow solid that remained. The dry yellow solid was washed with diethylether (200ml) and dried with oven at 60^0C for 1hour. It was then dissolved in water (200ml) and decolourizing charcoal (3g) was added. The solution was microwaved for 4minutes at 80% power level. It was then heated at 70^0C for 1hour, cooled and filtered. The filtrate was colourless. The water was removed and using lyophilizer. The resulting solid 1-butyl-1-methylpyrrolidinium chloride was then microwaved for 4minutes at 80% power level. It was then heated at 65^0C for 1hour and then cooled.

2.3. Preparation of solutions

The aggressive environment employed in the current study was made from a solution of analytical grade HCl (36% pure) with a specific gravity of 1.8 and distilled water using serial dilution approach. The varying concentrations of inhibited solutions were obtained by diluting 0.2 – 1.0 g of ionic liquid in 1L of 1.0 M HCl solution.

2.4. Weight loss measurement technique

Weight loss measurements were utilized to assess the inhibitive capabilities of the ionic liquid at five different temperatures: 303, 313, 323, 333, and 343 K. The metal coupons were placed in a 200 ml 1.0 M HCl test solution, with and without inhibitor, at varying concentrations (9×10^{-4} – 45×10^{-4} M). The amount of weight lost was calculated at various periods. After being removed from the test solution for five hours at one-hour increments, the coupons were submerged in acetone, cleaned under running water with a bristle brush, dried, and reweighed. The difference between the initial weight and the weight following the removal of the corrosion product was used to calculate the weight loss in grams. Equations (1), (2), and (3) were utilized to compute the degree of surface covering, DSC (θ), inhibitory efficiency (IE), and corrosion rate (CR), respectively.

$$CR = \frac{W_f - W_i}{At} \quad (1)$$

$$IE\ \% = \frac{W_0 - W_1}{W_0} \times 100 \quad (2)$$

$$DSC(\theta) = \frac{W_0 - W_1}{W_0} \quad (3)$$

where W_i and W_f are the initial and final weight of metal samples respectively; W_1 and W_0 are the weight loss values in presence and absence of inhibitor, respectively. A is the total area of the specimen and t is the immersion time and θ is the degree of surface coverage (El-Azzouzi *et al*, 2016).

2.5. Electrochemical method

The electrochemical tests were evaluated using electrochemical impedance spectroscopy (EIS) and potentiodynamic polarization measurements (PDP). A Princeton PAR-2273 model corrosion cylindrical cell with three electrodes was used for the electrochemical experiments. Graphite rod and a saturated calomel electrode (SCE) served as a counter and reference electrodes. The test solution, which functioned as the working electrode, was exposed to the mild steel samples that had a surface area of 1 cm^2 covered in epoxy gum. In order to get the steady state potential, electrochemical studies were conducted in aerated and stagnant conditions towards the end of the 1800s of dipping at 303 K. EIS studies were then carried out at corrosion potentials (E_{corr}) over a frequency range of 100 kHz–0.1 Hz; signal amplitude perturbation of 5 mV was used. A constant state open circuit potential was used for potentiodynamic polarization testing, which involved sweeping at potentials between -250 and +200 mV in relation to the corrosion potential. A constant scan rate of 0.5mV/s was used. Zsimpwin was used to analyze the EIS results. Equations (4) and (5) were used to determine the corrosion resistance effectiveness of the ionic liquid using data from electrochemical impedance spectroscopy and potentiodynamic polarization.

$$\eta_{pdp}(\%) = \frac{I_{corr(0)} - I_{corr(i)}}{I_{corr(0)}} \times 100 \quad (4)$$

$$\eta_{EIS}(\%) = \frac{R_{ct(i)} - R_{ct(0)}}{R_{ct(i)}} \times 100 \quad (5)$$

where $I_{corr(o)}$ and $I_{corr(i)}$ are the corrosion current density in the absence and presence of inhibitor respectively. $R_{ct(i)}$ and $R_{ct(o)}$ are charge transfer resistance in presence and absence of inhibitor respectively (Subsree and Selvi, 2020). Double-layer capacitance (C_{dl}) data were computed employing equation (6) (El-Hamadani *et al*., 2015; Subsree and Selvi, 2020).

$$C_{dl} = \frac{1}{2\pi f_{max} R_{ct}} \quad (6)$$

f_{max} represents the maximum frequency at which the imaginary impedance is highest.

2.6. Computational examination

Quantum chemical evaluations were performed with density functional theory (DFT) in the framework of the electronic structure program Dmol3, leveraging on a Mullikan population analysis as contained in the material studio 7.0 software (Accelrys, Inc.). Quantum chemical descriptors simulated and analyzed in this research include the following; lowest unoccupied molecular orbital (E_{LUMO}), energy of the highest occupied molecular orbital (E_{HOMO}), the energy gap (E_{LUMO}- E_{HOMO}),hardness (η), softness (σ), electron affinity (EA), ionization energy (IE), the absolute electronegativity(χ), electrophilicity (ω) and nucleophilicity (ε). These descriptors play vital role in evaluating the inhibition effectiveness of the ionic liquid (Haijaji *et al*., 2021). The ionization energy is estimated as the negative of the E_{HOMO}, while the negative of the E_{LUMO} equates to the electron affinity as shown in equations (7) and (8)

$$I = -E_{HOMO} \quad (7)$$

$$A = -E_{LUMO} \quad (8)$$

The electronegativity (χ), global hardness (***η***), and softness (σ) of inhibitor molecules were estimated using Equations (9), (10), and (11) (Nkuzinna *et al*., 2024).

$$\chi = \frac{\text{IE+EA}}{2} \quad (9)$$

$$\eta = \frac{IE-EA}{2} \quad (10)$$

$$\sigma = \frac{1}{\eta} \quad (11)$$

Electrophilicity and nucleophilicity were calculated using equations. (12) and (13)

$$\omega = \frac{\chi^2}{2\eta} \quad (12)$$

$$\varepsilon = \frac{1}{\omega} \quad (13)$$

A molecular dynamics (MD) simulation approach with the Forcite module, which is incorporated in Materials Studio 7.0 software, was used to assess the inhibitor's interaction and adsorption strength in relation to the aluminium surface. The computations were meticulously performed in a 10 x 8 supercell with a COMPASS force field and the smart algorithm with NVE (microcanonical) ensemble, a time step of 1.0 fs, and a simulation time of 5 ps. The temperature was set at 350k. Optimized structures of the ionic liquid and aluminium were utilized for the simulation. The system was doused every 250 steps. To accurately analyze the relationship between the molecules and the aluminum surface under study, the adsorption energy (E_{ads}) of the system was determined using equation (14).

$$E_{ads} = E_{total} - (E_{inh} + E_{Al}) \quad (14)$$

Where, E_{total}, E_{inh} and E_{Al} represent the energy of the single molecule, the Al slab without adsorption and the total energy of the system having the molecule and aluminium surface, respectively (Eziuka *et al*., 2023).

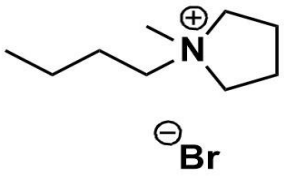
2.7. Structural characterization

The synthesised ionic liquid's functional groups were identified through the use of Fourier Transfer Infrared spectroscopy (Cary 630 model, Agilent Technologies, USA).

3.0 Results and Discussions

3.1 Structural characterization of 1-butyl – 1-methylpyrrolidinium bromide

Fourier transform infrared spectroscopy (FTIR) was employed to determine the functional groups in the ionic liquid. Figure 1 displays the FT-IR spectrum of the synthesized ionic liquid. The absorbance peak at 3365.8cm^{-1} relates to O-H stretching. The absorbance peaks at 2959.5cm^{-1}, 2933.4cm^{-1} 1 and 2873.8cm^{-1} indicate C-H bond stretching, 1461.1 cm^{-1} (ring C=C stretching), 1252.4 cm^{-1} (C-F stretching), 1110.7 cm^{-1}, 1073.5 cm^{-1} and 1028.7 cm^{-1} (C-O stretching), 1725.8 cm^{-1} and 1640.0 cm^{-1} (C=O stretching), 950.5 cm^{-1} (=C-H bending), 1215.1 cm^{-1} (=C-O-C symmetric and asymmetric stretching).



Scheme 1: 1-butyl-1-methylpyrrolidinium bromide with molecular weight of 222.17 g/mol

3.2. Weight loss measurement

3.2.1 Influence of ionic liquids concentrations

The influence of ionic liquid concentration on the metal corrosion in 1M HCl acidic solution at different inhibitor concentrations and temperatures are depicted in Table 1. Corrosion rate reduces when ionic liquid concentrations rise from 9 x 10^{-4} to 36 x 10^{-4}M, resulting in a significant increase in inhibitory efficacy. The inhibitory efficacy or protective strength of aluminium in the acidic environment containing 1M HCl increases with increasing inhibitor concentration. At 36 x 10^{-4}M inhibitor concentration in 1 M HCl, the greatest inhibition effectiveness values of 91.75% and 82.08% were achieved at 313K and 323K, respectively. The observed trend might be attributed to increasing adsorption and surface coverage as concentration increases, effectively isolating the metal surface from the medium (Verma *et al*., 2019). Based on Table 1, after 36 x 10^{-4}M inhibitor concentration, additional increases

resulted in a decline in the ionic liquid protective capability. At low concentrations, inhibitor molecules adsorb in flat or nearly flat orientations, resulting in maximal surface coverage due to dominating intermolecular attraction. At concentrations above the optimum, inhibitor molecules adsorb vertically, producing poor surface coverage due to intermolecular repulsion (Verma *et al*., 2019)

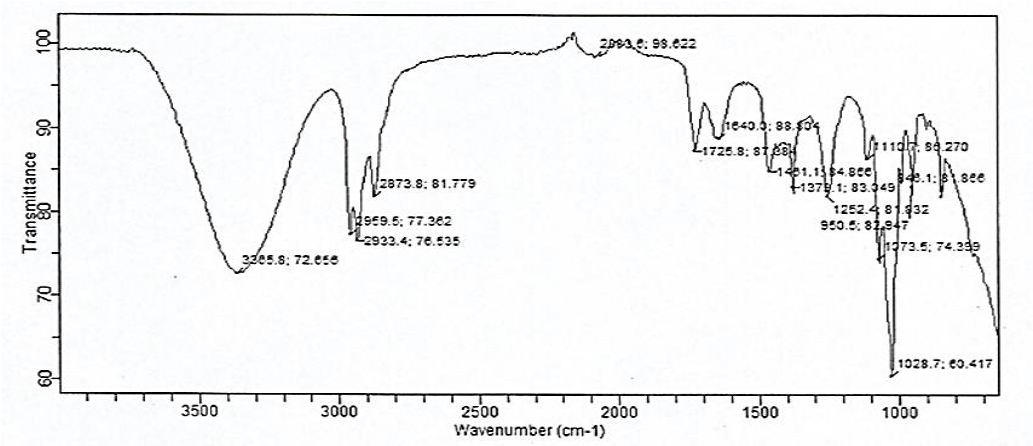


Figure 1. FT-IR spectrum of synthesized 1-butyl-1-methylpyrrolidinium bromide

Table 1: Weight loss estimates calculated for Aluminium in a 1.0 M HCl solution at various temperatures and concentrations

Temp (k)	Conc.(M)	CR(mg/cm^{2}hr)	DSC (θ)	IE(%)
	Blank	8.083	–	–
	9 x 10^{-4}	2.806	0.6529	65.29
313	18 x 10^{-4}	2.361	0.7079	70.79
	27 x 10^{-4}	1.361	0.8316	83.16
	36 x 10^{-4}	0.667	0.9175	91.75
	45 x 10^{-4}	0.944	0.8832	88.32
	Blank	8.528	–	–
323	9 x 10^{-4}	3.694	0.5668	56.68
	18 x 10^{-4}	3.194	0.6254	62.54
	27 x 10^{-4}	2.611	0.6938	69.38
	36 x 10^{-4}	1.528	0.8208	82.08
	45 x 10^{-4}	1.722	0.7980	79.80

3.2.2 Influence of time variations on corrosion and inhibition

Table 2 presents the experimental findings for corrosion parameters of aluminium in 1 M HCl without and with a 9 x 10^{-4} M inhibitor concentration for 5 hours at 313K. The findings showed that the inhibition efficiency rose with an increasing period of exposure between 1 and 4 hours but declined after 4 hours. The increase in inhibition efficacy with increasing immersion period is due to an increase in the amount of ionic liquid molecules adsorbing on the metal surface, which results in the formation of a more protective coating and, as a result, an increase in inhibition effectiveness. The highest inhibitory efficacy value obtained was 91.75%, which decreased to 88.47% after 5 hours. This is due to the loss of inhibitor molecules from the aluminium surface, which improves contact between the submerged metal and the HCl solution, leading the aluminium to corrode. The drop in inhibitory effectiveness after a long immersion period may be due to a reduction in the quantity of ionic liquid molecules present in the corrosive medium to prevent aluminium disintegration.

Table 2: Corrosion parameters of aluminium in 1.0M HCl solution in the blank and the presence of inhibitor concentration (9 x 10^{-4} M) at different immersion time

Conc.(g/L)	Time (h)	Weight loss (mg)	I.E (%)	CR (mg/cm^{2}hr)	DSC (θ)
	1	0.076	-	8.444	-
	2	0.111	-	6.167	-
Blank	3	0.157	-	5.815	-
	4	0.291	-	8.083	-
	5	0.295	-	6.556	-
	1	0.020	73.68	2.222	0.7368
	2	0.023	79.28	1.278	0.7928
9 x 10^{-4} M	3	0.022	85.19	0.815	0.8519
	4	0.024	91.75	0.667	0.9175
	5	0.034	88.47	0.756	0.8847

3.2.3 Temperature and kinetic effect investigation

The temperature effects on corrosion and inhibitor response of the ionic liquid in a 1M HCl environment (blank and with inhibitor concentrations of 4.5 x 10^{-4}M), for temperature variations in the range 303–343K, are presented in Table 3. The maximum corrosion rates for aluminum in 1M HCl in the blank solution are 7.861 mg/cm^{2}hr (303K), 8.083 mg/cm^{2}hr (313K), 8.528 mg/cm^2/hr. (323K), 8.722 mg/cm^{2}hr (333K), and 9.139 mg/cm^{2}hr (343K). Inhibitor-free solutions have a significantly higher corrosion rate than inhibitor-containing solutions, with inhibition efficiency increasing as temperature rises from 303K to 313K. Increased inhibitory strength with increased temperature implies chemical adsorption, which occurs owing to electron transfer or sharing between inhibitor molecules and the metal surface, most likely effecting both the anode and cathode sites. (Mobin *et al*., 2016; Aslam *et al*., 2020). The inhibition strengths decrease as temperatures rise between 313 and 343 K. This could be because chemical adsorption weakens at higher temperatures. The inhibitor molecules become highly energized, weakening their bond with the metal surface, as a result reduces the number of adsorbed inhibitor molecules, resulting in partial desorption (Aoun, 2017). In the inhibitor-free solution, the corrosion rate (9.139 mg/cm^{2}hr) peaked at 343K. However, when 4.5 x 10^{-4}M concentration of the inhibitor was added, the corrosion rate significantly decreased to 2.972mg/cm^2 hr., indicating a substantial reduction in the corrosion process.

Table 3: Temperature effect on aluminium in 1.0 M HCl solution in the blank and presence of 45 x 10^{-4} M at different temperatures

Conc.(M)	Temp (K)	Weight loss (mg)	CR (mg/cm^{2}hr)	I.E(%)	DSC (θ)
	303	0.283	7.861	–	–
	313	0.291	8.083	–	–
Blank	323	0.307	8.528	–	–
	333	0.314	8.722	–	–
	343	0.329	9.139	–	–
	303	0.035	0.972	87.63	0.8763
	313	0.024	0.667	91.75	0.9175
45 x 10^{-4}	323	0.055	1.528	82.08	0.8208
	333	0.078	2.167	75.16	0.7516
	343	0.107	2.972	67.48	0.6748

As previously stated, that temperature had a profound impact on the corrosion rate of the aluminium in the corrosive environment, with changes in temperature significantly influencing the rate of corrosion. The Arrhenius and transition state equations provide a useful framework for understanding the corrosion rate and temperature, offering valuable insights into how temperature influences the corrosion process. Plots of log CR versus 1/T and log (CR/T) versus 1/T for Arrhenius and transition state equations respectively for aluminium in 1M HCl are shown in Figure 2. The pertinent data are presented in Table 4. The Arrhenius and transition state equations are presented as equations (15) and (16) respectively (Anadebe *et al*., 2019; Onukwuli and Omotioma, 2019; Umoren *et al*., 2019).

$$\log(\mathrm{CR}) = \frac{-\mathrm{E_a}}{2.303\mathrm{RT}} + \log\mathrm{A} \quad (15)$$

$$\mathrm{Log}\left(\frac{\mathrm{CR}}{\mathrm{T}}\right) = \left[\log\left(\frac{\mathrm{R}}{\mathrm{Nh}}\right) + \left(\frac{\Delta \mathrm{S_a}}{2.303\mathrm{R}}\right)\right] - \frac{\Delta \mathrm{H_a}}{2.303\mathrm{RT}} \quad (16)$$

where, CR is the corrosion rate (mg/cm^{2}h), E_a is the activation energy (KJ/mol), R molar gas constant, T absolute temperature, A is the Arrhenius constant, h is plank's constant (6.626176 x 10^{-34}Js), N is Avagadro's number (6.02252 X 10^{23}mol^{-1}), ΔH_a is the enthalpy of activation and ΔS_a the entropy of activation. The results indicate that introducing the inhibitor to the acid solution increases the activation energy value, indicating a heightened energy barrier for the corrosion process. This suggests that as the inhibitor concentration increases, the energy required for corrosion to occur also increases, making it more difficult for corrosion to take place. Figure 2 reveals a similar trend between the apparent activation energy (E_a) and the apparent enthalpy of activation (ΔH_a), which may be expressed by the equation: $\Delta H_a = E_a - RT$. The corrosion process has a positive ΔH_a, meaning it is an endothermic process that requires energy input to reach the activated state, making it more energetically demanding to initiate the corrosion reaction (Umoren *et al*., 2019; Laamari *et al*., 2016). The higher E_a and ΔH_a values in the ionic liquid-containing solution compared to the uncontrolled acid solution reveal that the adsorption of inhibitor molecules onto the aluminium surface changes the corrosion mechanism, leading to an increased energy barrier and a slowed corrosion rate. Furthermore, the entropy of activation (ΔS_a) value in the presence of the inhibitor is higher compared to the blank, indicating that the increased randomness or disorder is a result of the competitive adsorption between water molecules and the ionic liquid inhibitor, leading to a more disordered transition state (Feng *et al*., 2019).

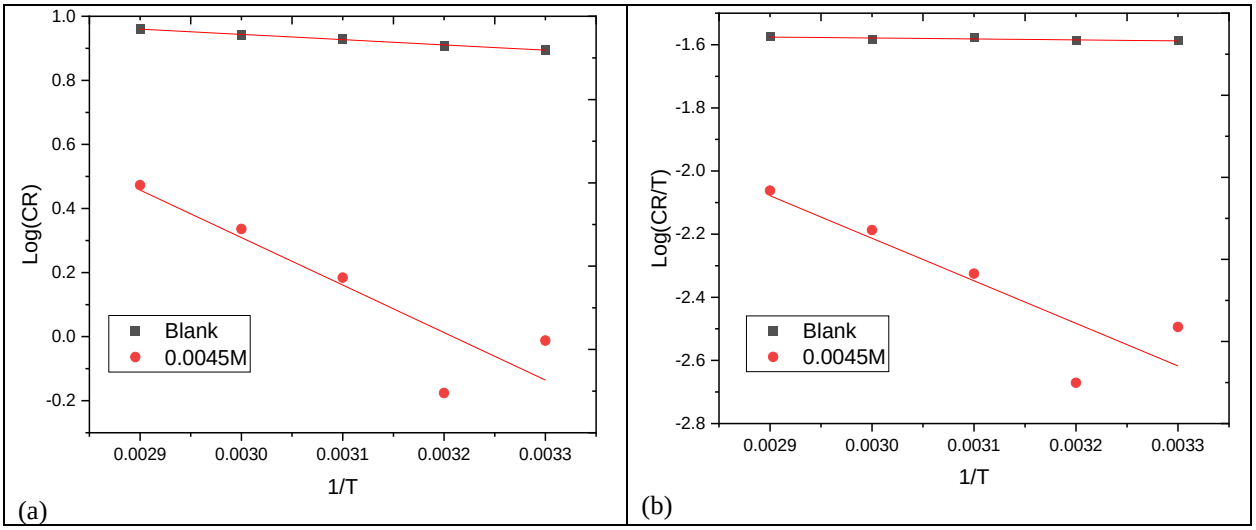


Figure 2: (a) Arrhenius plots and (b) transition state plots for the corrosion of aluminium in 1 M HCl in the blank and presence of [BMPyr]Br.

Table 4: Results of the kinetic and activation data for the corrosion of aluminium in 1.0 M HCl in the blank and presence of [BMPyr]Br

	Fig 2a		Fig 2b				
Solution (M)	**Slope**	**Intercept**	**Slope**	**Intercept**	**E_a (J/mol)**	**ΔH_a(J/mol**	**ΔS_a(J/mol)**
Blank	-164.00	1.4355	-3.00	-1.3886	3140	57.44	-226.078
45x10^{-4}	-1482.5	4.7567	-1348	1.831	28385	25810.35	-162.517

3.2.4 Surface interaction consideration

Elucidating the mechanism of how the inhibitor interacts with the metal surface necessitates an understanding of the adsorption isotherms, which reveals the equilibrium behaviour of inhibitor molecules on the surface and how they bind to it (Gupta *et al*., 2016). Adsorption laws, such as the Langmuir, Temkin, Frumkin, and Florry-Huggins isotherms, are employed to fit surface coverage (θ) values at varying inhibitor doses. The isotherms reveal that surface coverage (θ) is connected to inhibition concentration by the following equations.

$$\frac{\mathrm{C}}{\theta} = \frac{1}{\mathrm{K_{ads}}} + \mathrm{C} \text{ (Langmuir)} \quad (17)$$

$$\exp(-2\alpha\theta) = \mathrm{K_{ads}C_{inh}} \text{ (Temkins)} \quad (18)$$

$$\left(\frac{\theta}{1-\theta}\right)\exp(2\alpha\theta) = K_{ads}C_{inh}(\text{Frumkins}) \quad (19)$$

$$\log\frac{C}{\theta} = \log K_{ads} + \times \log(1-\theta)(\text{Flory-Huggins}) \quad (20)$$

where K_{ads} is the equilibrium constant for the adsorption process, C_{inh} is the inhibition concentration, θ is the surface coverage, α is the lateral interaction parameter and x is the constant associated with the number of molecules of water displaced and/or the number of adsorbed inhibitor molecules (El-Hamadani *et al*., 2015; Ejikeme *et al*., 2015; Qiang *et al*., 2017; Pancharatna et al., 2019). The linear regression coefficient (R^2) was employed to assess which adsorption isotherm model most accurately represented the experimental data, enabling the identification of the best fit isotherm. The experimental data was best described by an adsorption isotherm with R^2 approaching unity (Al-Azawi *et al*., 2018; Madkour *et al*., 2018). The Langmuir adsorption isotherm was found to be most suitable, with an excellent fit to the experimental data, as evidenced by high R^2 values of 0.9893 at 313K and 0.9873 at 323K, indicating a strong correlation between the model and the data at both temperatures. Adsorption isotherm plots and the accompanying thermodynamic parameters are given in Figure 3 and Table 5, respectively. The intercept values from the Langmuir plots were used to calculate the adsorption constant (K_{ads}) by taking their reciprocals. Then the values of the standard Gibbs free energy (ΔG_{ads}) were determined by substituting the calculated K_{ads} values into equation (21)

$$K_{ads} = \frac{1}{55.5}\exp\left[\frac{-\Delta G_{ads}}{RT}\right] \quad (21)$$

where 55.5 is in mol dm^{-3} and is the molar concentration of water in the solution, R is the universal gas constant, and T is the temperature in Kelvin (El-Haijaji *et al*., 2019; Ma *et al.*, 2016). Table 5 displays the intercept, adsorption equilibrium constant (K_{ads}), correlation coefficient (R^2), and free energy of adsorption (ΔG_{ads}) data. The ΔG_{ads} has well-defined boundaries; -20KJ/mol for physisorption and -40KJ/mol or higher for chemisorption. Values within this range suggest a hybrid adsorption mechanism, where both physical and chemical interaction occur concurrently on the metal surface (Shetty and Shetty, 2017). The values of ΔG_{ads} are negative and are -29.845KJ/mol and -30.371KJ/mol for 313K and 323K respectively. The fact that ΔG_{ads} values are negative indicates that the adsorption of the inhibitor onto the aluminium surface occurs spontaneously, meaning that it is a thermodynamically favourable process that can occur naturally without the need for external energy input. Additionally, it is evident that as temperature rises, the K_{ads} value decreases, indicating a weakening of the adsorption bond between the inhibitor and the metal surface, leading to a decline in adsorption efficiency and protective effect (Solomon *et al*., 2020).

Table 5: Results of co-efficient of linear regression of adsorption isotherm plots and thermodynamic parameters

Adsorption Isotherm	Temperature (K)	R^2	K	ΔG_{ads} (KJ/mol)	Isotherm property	
Langmuir Isotherm	313	0.9893	1724.14	-29.845		
	323	0.9873	1470.69	-30.371		
Temkim isotherm	313	0.8983	43401.03	-38.246	a	-2.9231
	323	0.8944	32114.41	-38.659		-3.0830
Frumkin Isotherm	313	0.9867	0.0023	5.385	α	2.5702
	323	0.9765	0.0044	3.775		2.2707
Flory-Huggins Isotherm	313	0.7420	1161.61	-28.823	x	0.7089
	323	0.7522	1188.86	-29.806		1.0998

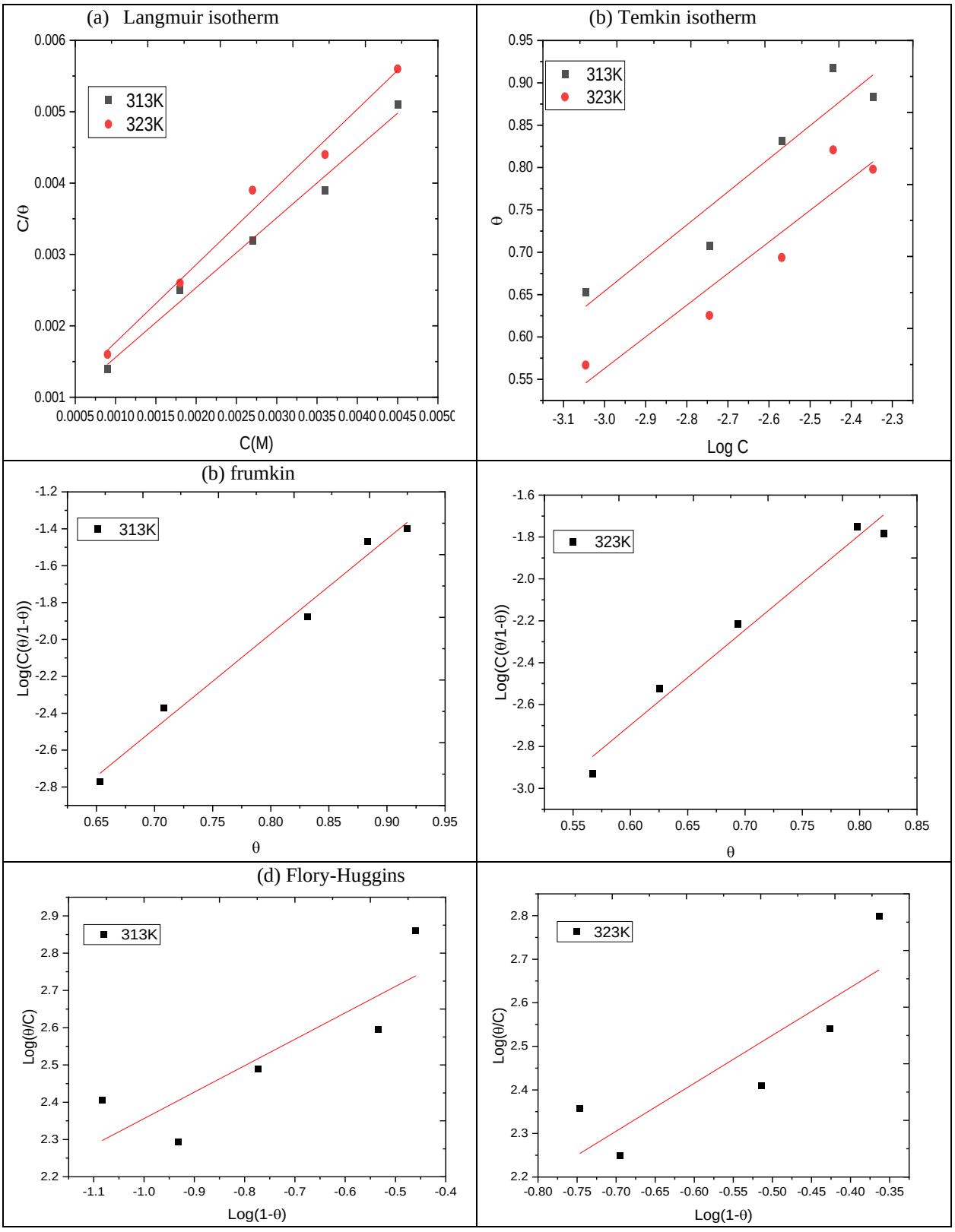


Figure 3: Adsorption isotherm plots of IL on aluminium: (a) Langmuir isotherm; (b) Temkins isotherm; (c) Frumkins isotherm; (d) Flory-Huggins isotherm.

3.3 Electrochemical assessment

3.3.1 Impedance spectroscopy (EIS) analysis

Nyquist and Bode plots of aluminium in 1.0MHCl in various concentrations of ionic liquid are given in Figures 4a and 4b, revealing three clear loops that illustrate the connection between real and imaginary impedance components. The consistent shape of the capacitance arcs suggests a uniform charge transfer process through dissolution, unaffected by inhibitor molecules (Dehghani *et al*., 2019; Qiang *et al*., 2021). The Nyquist plot shows a larger capacitive loop for the ionic liquid containing solution compared to the blank, and the loop size increases with rising ionic liquid concentration. This indicated that the ionic liquid presence slows down the charge transfer between the aluminium and the solution, leading to reduced corrosion (Wang *et al*., 2020).

The Bode magnitude plots indicate that higher ionic liquid concentrations results in a substantial increase in low-frequency impedance module (Z_{mod}), suggesting improved corrosion protection. Moreover, the phase angle values demonstrate that the ionic liquid significantly enhances the natural protective barrier of aluminium with increasing ionic liquid concentrations, leading to further enhancements in the corrosion resistance. The data in Table 6 shows that increasing the ionic liquid concentration leads to an increase in charge transfer resistance (R_{ct}), suggesting the development of protective coating on the aluminium surface. This coating forms a denser surface film which acts as a barrier to slow down the penetration of corrosive species, resulting in improved corrosion resistance. The ionic liquid achieves a remarkable inhibition efficiency of 89.99% with $45x10^{-4}$M ionic liquid concentration, demonstrating a pronounced inhibitory effect resulting from its adsorption onto the aluminium surface. Furthermore, the increase in inhibitor concentration leads to a significant reduction in electric double layer capacitance (C_{dl}) compared to the inhibitor-free solution.

This indicates that inhibitor molecules replace water molecules on aluminium surface creating a thicker protective layer that reduces the interaction between the aluminium and the corrosive solution (Wang *et al*., 2020). The error reference source not found (N) values in Table 6 reveal that in the absence of inhibitor, the aluminium surface exhibits heterogeneity (N= 0.88), indicating the presence of surface defects, such as contaminants, surface roughness, lattice imperfection, , size and uneven distribution of active sites, and other surface flaws (Arellanes-lozada *et al*., 2018). The presence of the ionic liquid leads to slight increase in N values compared to the bank, indicating that the ionic liquid molecules improve the surface homogeneity of aluminium. This suggests that the ionic liquid forms an adsorptive layer on the aluminium surface, reducing surface imperfection and defects, and thereby enhancing corrosion protection (Nkuzinna *et al*., 2024).

Table 6: EIS data of aluminium corrosion in 1M HCl solution in the blank and presence of [BMPyr]Br

Conc.(M)	R_S (Ωcm^2)	R_{ct} (Ω/cm^2)	N	C_{dl} (μFCm^{-2})	-θ	% IE
Blank	1.678	188.6	0.88	8.44	58.5	–
9×10^{-4}	1.736	597.4	0.89	2.66	66.5	68.4
45×10^{-4}	1.823	952.7	0.89	1.67	74.0	80.2

Table 7: PDP data of aluminium corrosion in 1.0 M HCl solution in the blank and presence of [BMPyr]Br

Conc.(M)	E_{corr}(mV)	I_{corr}($\mu A/cm^2$)	Θ	I.E (%)
Blank	-482.6	145.8	–	–
9×10^{-4}	-472.6	29.3	0.799	79.90
45×10^{-4}	-458.4	14.7	0.899	89.99

3.3.2 Potentiodynamic polarization (PDP) analysis

The PDP curves in Figure 7 show the effect of the inhibitor on aluminium corrosion in 1M HCl solution. The presence of inhibitor leads to a substantial decrease in corrosion current density (I_{corr}) observed in both the cathodic and anodic region, indicating a reduction in corrosion rate compared to the blank solution without inhibitor. The finding suggests that the inhibitor exerts a suppressive effect on both the reduction (cathodic) and oxidation (anodic) reactions involved in the corrosion process. Based on this behaviour, this compound can be categorized as a mixed-type inhibitor with a predominantly effect on the cathodic reaction (Shaban *et al*., 2021). Table 7 displays the electrochemical kinetic parameter values obtained from polarization curves. The corrosion current density decreases significantly as the inhibitor concentration increases, indicting a corresponding in corrosion rate. Notably, the highest I_{corr} value 145.8$\mu A/cm^2$occurs in the inhibitor-free solution. This implies that as the inhibitor concentration increases, more inhibitor molecules are available to cover the metal surface, resulting in a greater surface area being occupied by the inhibitor. The inhibition efficiency improves with increasing inhibitor concentration, indicating a

dose-dependent response. This is likely because high concentration of inhibitor molecules result in a more extensive and complete coverage of aluminium surface, maximizing corrosion protection. . The difference in corrosion potential (E_{corr}) between the inhibitor-treated system and the acid blank is less than $\pm 85mV$. This suggests that the ionic liquid under investigation is a mixed-type inhibitor.

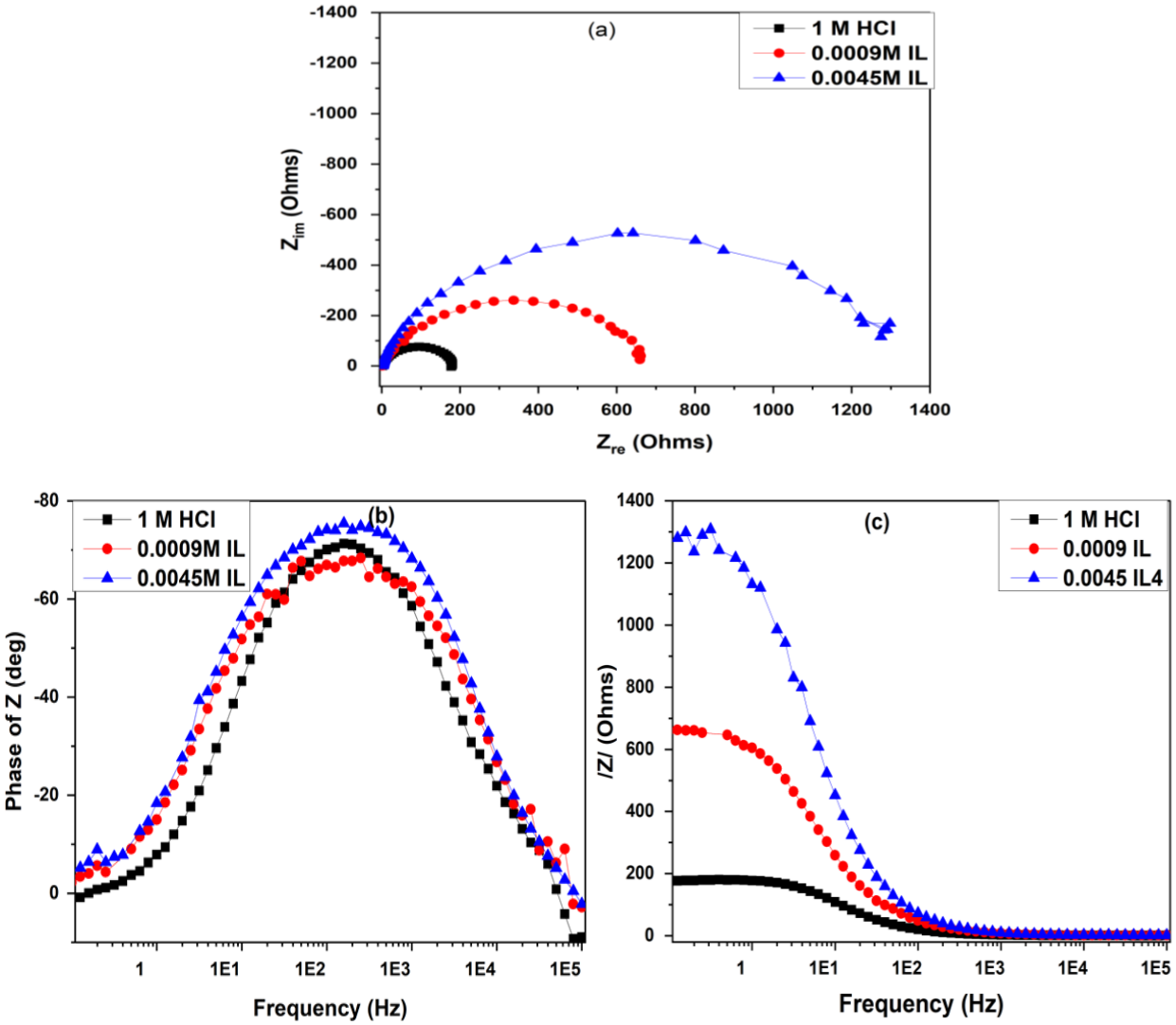


Figure 4: Electrochemical impedance spectra of aluminium in: (a) Nyquist and (b) Bode phase angle and (c) Bode modulus plots in 1 M HCl environment in the absence and presence of different concentrations of [BMPyr]Br.

3.4 Computational analysis

3.4.1 Theoretical chemical analysis

Density Functional Theory (DFT) computational modelling acts as theoretical framework for understanding the relationship between the molecular structure of corrosion inhibitors and their inhibitory effectiveness, enabling the correlation of inhibitor efficiency with their electronic properties. The quantum chemical parameters listed in Table 8 are metrics used to assess molecular reactivity The energy of highest occupied molecular orbital (E_{HOMO}) of an inhibitor serves as an indicator of an inhibitor's capacity to donate electrons to the empty orbitals of metal atoms, facilitating interactions that lead to adsorption and subsequent reduction of corrosion. Previous research has shown that a high E_{HOMO} value indicates a greater likelihood of a molecule to act as an electron donor, readily transferring electrons to a specific empty molecular orbital (Pancharatna *et al*., 2019). In this case, the value of -4.678eV is within the context considered to be relatively high indicating a high tendency to donate electron. The energy of lowest occupied molecular orbital (E_{LUMO}) of an inhibitor determines its electron- accepting capacity, showing how

readily it can receive electrons from metal atoms, which affects its chemical reactivity and ability to form a protective film, hindering corrosion. A low E_{LUMO} value (-1.288eV) indicates that [BMPyr]Br can easily accept electron from the metal surface and ensure high inhibition efficacy (Benhiba *et al*., 2020; Lgaz *et al*., 2017). The energy gap (ΔE) is the difference between the E_{HOMO} and the E_{LUMO}. Inhibitor molecules with large energy difference are extremely stable and inert, resisting chemical interactions, while molecules with small energy difference are highly reactive and prone to chemical interactions, making then more likely to participate in corrosion inhibiting reactions (Aslam *et al*., 2020). The small energy gap value (3.39eV) of [BMPyr]Br makes it easier for the inhibitor to adsorb on the aluminium surface, enhancing its corrosion-inhibiting properties. The optimized structures, graphical images of frontier molecular orbitals (HOMO and LUMO) for the ionic liquids are shown in Figure 6.

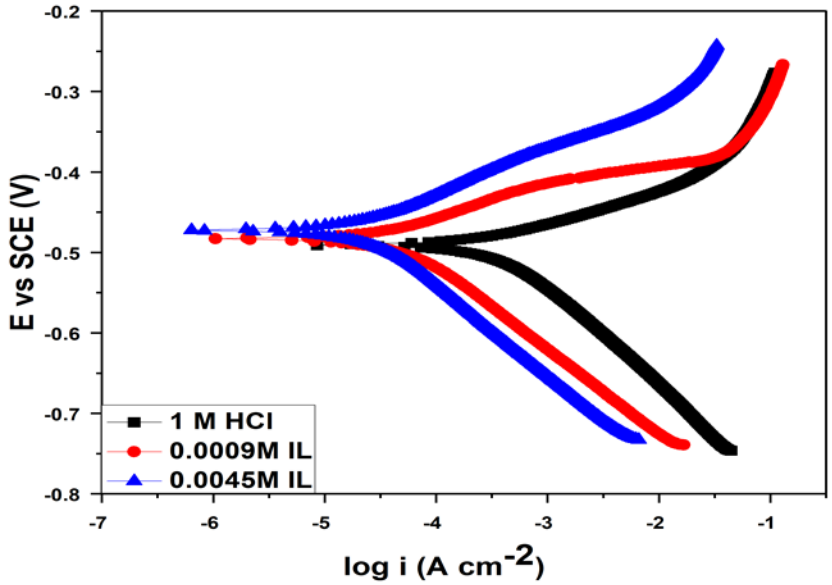


Figure 5: Potentiodynamic polarization curves of aluminium in 1 M HCl in the absence and presence of [BMPyr]Br

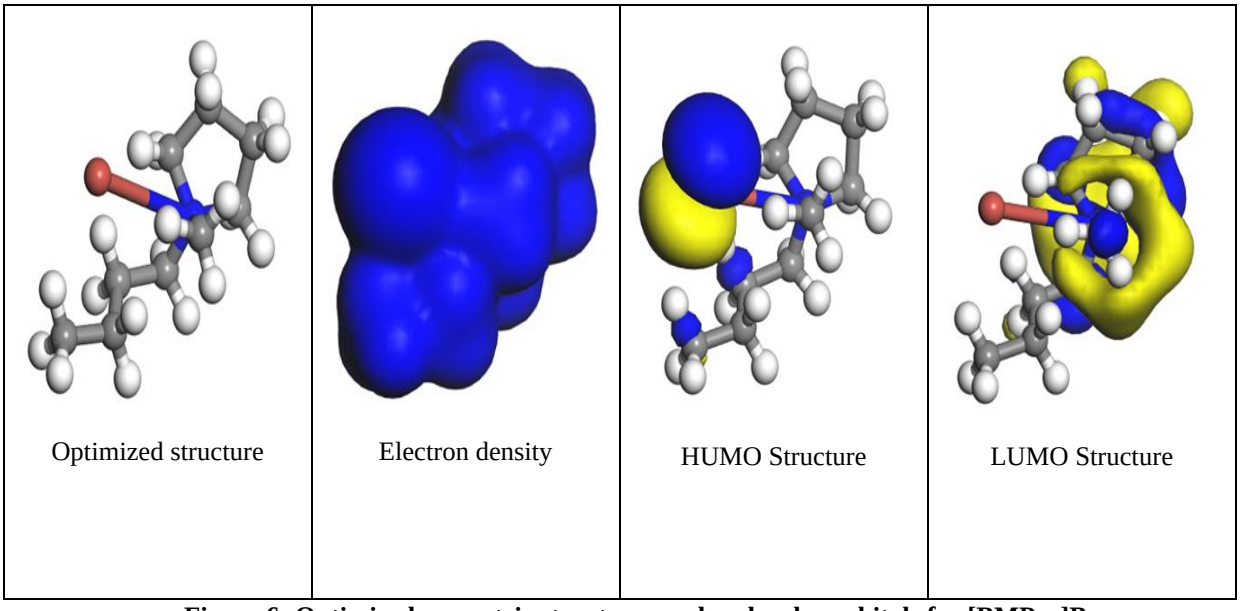


Figure 6: Optimized geometric structures and molecular orbitals for [BMPyr]Br

The global hardness (***η***) and softness (σ) are metrics used to assess molecular reactivity. These values are derived from the E_{HOMO} and E_{LUMO} energies and provide a measure of the molecule's ability to engage in chemical reactions. A molecule's reactivity is inversely related to its global hardness, with soft molecules (low global hardness) being more reactive and capable of easily donating electrons whereas hard molecules (high global hardness) are less reactive and more resistant to electron transfer, making them less likely to engage in chemical reactions (Sasikumar *et al*., 2015). Electronegativity (χ) is a measure of a molecule's reactivity, specifically its tendency to attract and retain electrons. A high electronegativity value indicates a molecule's strong electron-withholding ability, whereas a low electronegativity value indicates a greater willingness to release electrons and form bond with other molecules. The electrophilicity index (ω) measures a molecule's ability to accept electros, indicating its electron-accepting capacity and its tendency to form bonds with electron denoting molecules. Table 8 presents the electrophilicity index of the ionic liquid, which reveals its electron-accepting ability. A higher electrophilicity value indicates a greater capacity to accept electron, making the molecule more electron-hungry and reactive, while a lower value indicates a lesser ability to accept electrons.

Table 8. Quantum chemical parameters from Density functional theory (DFT)

S/N	Parameters	Values
1	E_{HOMO} (eV)	-4.678
2	E_{LUMO} (eV)	-1.288
3	ΔE (eV)	3.390
4	Ionization energy I (eV)	4.678
5	Electron affinity A (eV)	1.288
6	Hardness (***ŋ***)	1.695
7	Softness (σ)	0.590
8	Electronegativity (χ)	2.983
9	Electrophilicity (ω)	2.625
10	Nucleophilicity (ε)	0.381

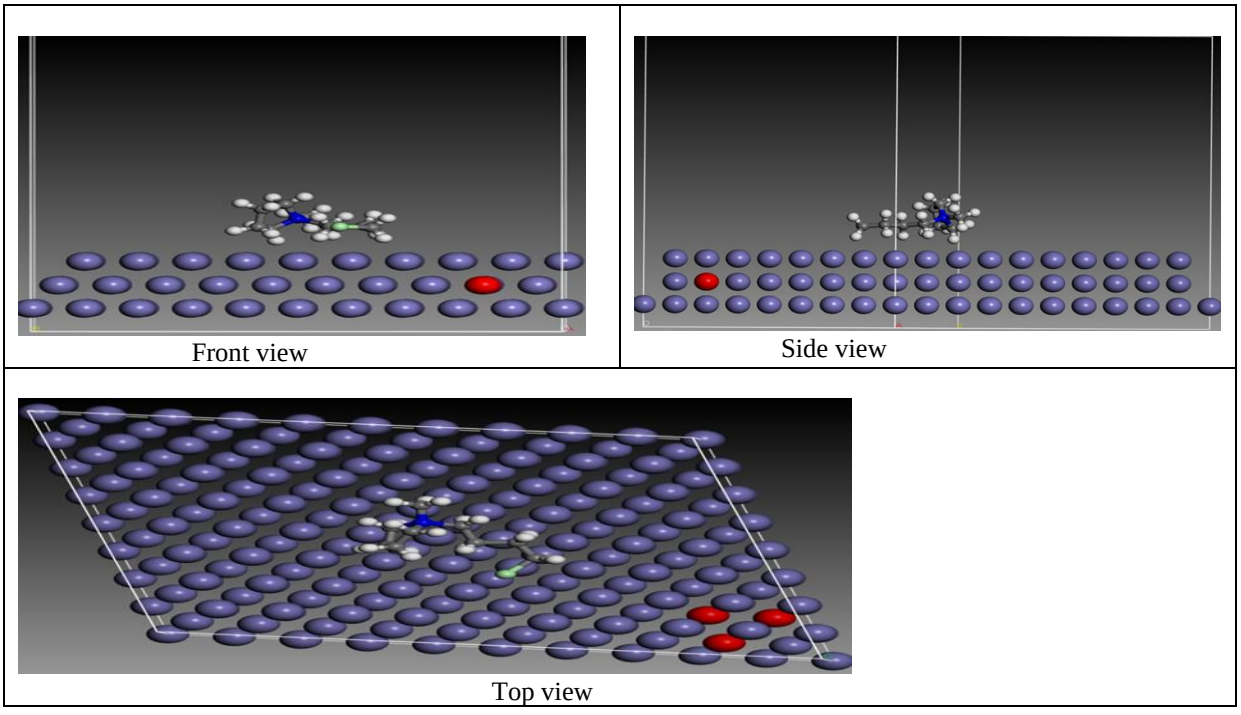


Figure 7: Stable adsorption configuration of [BMPyr]Br

3.4.2 Simulation of molecular interactions and dynamics

Simulations of molecular dynamics reveals the intricate interactions between corrosion inhibitors and metal surfaces in diverse environments, helping to understand how these molecules prevent corrosion and protect metals (Verma *et*

al.,2019). Figure 7 provides the optimal arrangements of inhibitor molecules on the aluminium surface from multiple angles (front, side, and top views), highlighting the stable configurations achieved through adsorption. The proximity of the inhibitor molecules to the surface in all cases implies a strong adsorption onto the aluminium surface, which is crucial for achieving excellent corrosion protection. The adsorption of the ionic liquid on the metal surface occurs in a parallel fashion, with the molecules lying flat and parallel to each other. Table 9 presents the energy values for two key descriptors, interaction energy ($E_{interaction}$) and binding energy ($E_{binding}$). The negative interaction energy of [BMPyr]Br indicates that the adsorption process is thermodynamically favourable, meaning the adsorption can occur spontaneously, without the need for external energy, indicating a strong affinity between the chemical species and the metal surface (Asadi *et al*., 2019; Sigh *et al*., 2021). The $E_{binding}$ represents the amount of energy needed to break the bonds between the inhibitor molecules and the aluminium surface, effectively removing the inhibitor from the surface (Haris *et al*., 2020). The high positive value $E_{binding}$ of [BMPyr]Br shows a strong attractive force between the inhibitor and the aluminium surface and hence a high inhibition efficiency.

Table 9: $E_{interaction}$ and $E_{binding}$ energies for [BMPyr]Br on the metal surface

Parameters	Values
$E_{interaction}$ (KJ/mol)	94
$E_{binding}$ (KJ/mol)	-94

4.0. Conclusion

The inhibitory effects of 1-butyl-1-methylpyrrolidinium bromide on aluminium corrosion in a 1MHCl solution were comprehensively evaluated using a multi- technique approach, including weight loss, electrochemical, and computational analysis methods. The experimental findings lead to the following conclusions.

1. The newly synthesized ionic liquid shows remarkable corrosion inhibition efficacy for aluminium against corrosion in a 1MHCl environment.
2. The ionic liquid showed its highest corrosion efficiency of 91.75% at 313K and a lower efficiency of 67.48% at 343K for the same inhibitor concentration, indicating that temperature significantly influences the corrosion process.
3. The data indicates that the corrosion inhibition efficiency improves as the concentration of [BMPyr]Br increases, reaching a maximum efficiency at a concentration of 36 x 10^{-4}M.
4. The inhibition effectiveness increases with time of immersion, reaching its peak at 4hrs.
5. The Langmuir adsorption isotherm accurately describes the adsorption of the ionic liquid onto the aluminium surface. Additionally the Gibbs energy value reveals that the adsorption process involves a combination both physical and chemical mechanism.
6. The results of the potentiodynamic polarization experiment revealed that the ionic liquid functions as a mixed-type inhibitor, with a dominant effect on the cathodic reaction.
7. The experimental and theoretical findings (from DFT and MD) are in perfect accord, providing robust evidence that the ionic liquid is a highly effective corrosion inhibitor, with all approaches converging to a consistent conclusion.

Acknowledgement

This research was supported by Federal University of Technology Owerri, Imo State Nigeria through the Tetiary Education Fund (TETFUND) in providing the necessary financial support.

Conflict of interest

The authors state that they have no known conflicting financial or personal interests that might have influenced the work presented in this study.

References

Abbas, M. A., Zakaria, K., El-Shamy, A. M., & Abedin, S. Z. E. (2021). Utilization of 1-butylpyrrolidinium chloride ionic liquid as an eco-friendly corrosion inhibitor and biocide for oilfield equipment: combined weight loss, electrochemical and SEM studies. Zeitschrift für Physikalische Chemie, 235(4), 377-406.

Al-Azawi, K. F., Mohammed, I. M., Al-Baghdadi, S. B., Salman, T. A., Issa, H. A., Al-Amiery, A. A., ...

&Kadhum, A. A. H. (2018). Experimental and quantum chemical simulations on the corrosion inhibition of mild steel by 3-((5-(3, 5-dinitrophenyl)-1, 3, 4-thiadiazol-2-yl) imino) indolin-2-one.*Results in Physics*, *9*, 278-283.

Anadebe, V. C., Onukwuli,O. D., Omotioma, M., &Okafor, N. A. (2019). Experimental, theoretical modelling and optimization of inhibition efficiency of pigeon pea leaf extract as anti-corrosion agent of mild steel in acid environment. *Materials Chemistry and Physics, 233*, 120-132.

Aoun, S. B. (2017). On the corrosion inhibition of carbon steel in 1 M HCl with a pyridinium-ionic liquid: chemical, thermodynamic, kinetic and electrochemical studies.RSC advances, 7(58), 36688-36696.

Arellanes-Lozada, P., Olivares-Xometl, O., Likhanova, N. V., Lijanova, I. V., Vargas-García, J. R., & Hernández-Ramírez, R. E. (2018). Adsorption and performance of ammonium-based ionic liquids as corrosion inhibitors of steel. Journal of Molecular Liquids, 265, 151-163.

Asadi, N., Ramezanzadeh, M., Bahlakeh, G., & Ramezanzadeh, B. (2019). Utilizing Lemon Balm extract as an effective green corrosion inhibitor for mild steel in 1M HCl solution: A detailed experimental, molecular dynamics, Monte Carlo and quantum mechanics study. *Journal of the Taiwan Institute of Chemical Engineers*, *95*, 252-272.

Aslam, R., Mobin, M., Obot, I. B., &Alamri, A. H. (2020). Ionic liquids derived from α-amino acid ester salts as potent green corrosion inhibitors for mild steel in 1M HCl. *Journal of Molecular Liquids*, *318*, 113982.

Atta, A. M., El-Mahdy, G. A., Allohedan, H. A., & Abdullah, M. M. (2016). Adsorption characteristics and corrosion inhibition efficiency of ethoxylatedoctadecylamine ionic liquid in aqueous acid solution. Int. J. Electrochem. Sci, 11, 882-898.

Benhiba, F., Hsissou, R., Benzekri, Z., Belghiti, M. E., Lamhamdi, A., Bellaouchou, A., ... & Zarrouk, A. (2020). Nitro substituent effect on the electronic behavior and inhibitory performance of two quinoxaline derivatives in relation to the corrosion of mild steel in 1M HCl. *Journal of Molecular Liquids*, *312*, 113367.

Byrne, A., Holmes, N., & Norton, B. (2016). State-of-the-art review of cathodic protection for reinforced concrete structures. *Magazine of Concrete Research*, *68*(13), 664-677.

Cao, S., Liu, D., Ding, H., Lu, H., & Gui, J. (2020). Towards understanding corrosion inhibition of sulfonate/carboxylate functionalized ionic liquids: an experimental and theoretical study. *Journal of Colloid and Interface Science*, *579*, 315-329.

Cao, S., Liu, D., Ding, H., Wang, J., Lu, H., &Gui, J. (2019). Task-specific ionic liquids as corrosion inhibitors on carbon steel in 0.5 M HCl solution: an experimental and theoretical study. Corrosion Science, 153, 301-313.

Dehghani, A., Bahlakeh, G., & Ramezanzadeh, B. (2019). A detailed electrochemical/theoretical exploration of the aqueous Chinese gooseberry fruit shell extract as a green and cheap corrosion inhibitor for mild steel in acidic solution. Journal of Molecular Liquids, 282, 366-384.

Dermani, A. K., Kowsari, E., Ramezanzadeh, B., &Amini, R. (2019). Utilizing imidazole based ionic liquid as an environmentally friendly process for enhancement of the epoxy coating/graphene oxide composite corrosion resistance. J. Ind. Eng. Chem., 79, 353-363.

Deyab, M. A. (2020). Understanding the anti-corrosion mechanism and performance of ionic liquids in desalination, petroleum, pickling, de-scaling, and acid cleaning applications. *Journal of Molecular Liquids*, *309*, 113107.

Deyab, M. A., Zaky, M. T., & Nessim, M. I. (2017). Inhibition of acid corrosion of carbon steel using four imidazolium tetrafluoroborates ionic liquids. *Journal of Molecular Liquids*, *229*, 396-404.

Ejikeme, P. M., Umana, S. G., Menkiti, M. C., &Onukwuli, O. D. (2015). Inhibition of mild steel and aluminium corrosion in 1M H_2SO_4 by leaves extract of African breadfruit. *International Journal of Materials and Chemistry*, *5* (1), 14-23.

El Azzouzi, M., Aouniti, A., Tighadouin, S., Elmsellem, H., Radi, S., Hammouti, B., ...&Zarrouk, A. (2016). Some hydrazine derivatives as corrosion inhibitors for mild steel in 1.0 M HCl: weight loss, electrochemichal, SEM and theoretical studies. *Journal of Molecular Liquids*, *221*, 633-641.

El Hamdani, N., Fdil, R., Tourabi, M., Jama, C., &Bentiss, F. (2015). Alkaloids extract of Retamamonosperma (L.) Boiss.seeds used as novel eco-friendly inhibitor for carbon steel corrosion in 1 M HCl solution: Electrochemical and surface studies. *Applied Surface Science*, *357*, 1294-1305.

El-Hajjaji, F., Messali, M., de Yuso, M. M., Rodríguez-Castellón, E., Almutairi, S., Bandosz, T. J., &Algarra, M. (2019). Effect of 1-(3-phenoxypropyl) pyridazin-1-ium bromide on steel corrosion inhibition in acidic medium.*Journal of colloid and interface science*, *541*, 418-424.

El-Katori, E. E., & Abousalem, A. S. (2019). Impact of some pyrrolidinium ionic liquids on copper dissolution behavior in acidic environment: experimental, morphological and theoretical insights. RSC advances, 9(36), 20760-20777.

El-Saeed, H. M., Fouda, A. S., Deyab, M. A., Shalabi, K., Nessim, M. I., & El-Katori, E. E. (2022). Synthesis and characterization of novel ionic liquids based on imidazolium for acid corrosion inhibition of aluminum: Experimental, spectral, and computational study. *Journal of Molecular Liquids*, *358*, 119177.

El-Shamy, A. M., Zakaria, K., Abbas, M. A., & El Abedin, S. Z. (2015). Anti-bacterial and anti-corrosion effects of the ionic liquid 1-butyl-1-methylpyrrolidinium trifluoromethylsulfonate. Journal of Molecular Liquids, 211, 363-369.

Eziuka J. E., Onyeachu B. I., Njoku D. I., Nwanonenyi S. C., Chidiebere M.A., Oguzie E.E. (2023). Elucidating the inhibition behaviour of Pterocarpussantalinoides leaves extract on mild steel corrosion in H_2SO_4 solution–GC-MS, FTIR, SEM, Experimental and computational approach. Mor. J. Chem., 11(03), 579-896. doi.org/10.48317/IMIST.PRSM/morjchemv11i03.39198

Feng, L., Zhang, S., Lu, Y., Tan, B., Chen, S., & Guo, L. (2019). Synergistic corrosion inhibition effect of thiazolyl-based ionic liquids between anions and cations for copper in HCl solution. *Applied Surface Science*, *483*, 901-911.

Gupta, N. K., Verma, C., Quraishi, M. A., & Mukherjee, A. K. (2016). Schiff's bases derived from l-lysine and aromatic aldehydes as green corrosion inhibitors for mild steel: experimental and theoretical studies. Journal of Molecular Liquids, 215, 47-57.

Hajjaji, F. E., Salim, R., Ech-chihbi, E., Titi, A., Messali, M., Kaya, S., ...&Taleb, M. (2021). New imidazolium ionic liquids as ecofriendly corrosion inhibitors for mild steel in hydrochloric acid (1 M): Experimental and theoretical approach. Journal of the Taiwan Institute of Chemical Engineers, 123, 346-362.

Haris, N. I. N., Sobri, S., Yusof, Y. A., & Kassim, N. K. (2020). An overview of molecular dynamic simulation for corrosion inhibition of ferrous metals. *Metals*, *11*(1), 46.

Kobzar, Y. L., & Fatyeyeva, K. (2021). Ionic liquids as green and sustainable steel corrosion inhibitors: Recent developments. *Chemical Engineering Journal*, *425*, 131480.

Laamari, M. R., Benzakour, J., Berrekhis, F., Derja, A., & Villemin, D. (2016). Adsorption and corrosion inhibition of carbon steel in hydrochloric acid medium by hexamethylenediamine tetra (methylene phosphonic acid). *Arabian Journal of Chemistry*, *9*, S245-S251.

Lgaz, H., Salghi, R., Bhat, K. S., Chaouiki, A., & Jodeh, S. (2017). Correlated experimental and theoretical study on inhibition behavior of novel quinoline derivatives for the corrosion of mild steel in hydrochloric acid solution. *Journal of Molecular Liquids*, *244*, 154-168.

Likhanova, N. V., Arellanes-Lozada, P., Olivares-Xometl, O., Lijanova, I. V., Arriola-Morales, J., Mendoza-Hérnandez, J. C., & Corro, G. (2019). Ionic liquids with carboxylic-acid-derived anions evaluated as corrosion inhibitors under dynamic conditions. *Int. J. Electrochem. Sci*, *14*, 2655-2671.

Ma, Y., Han, F., Li, Z., & Xia, C. (2016). Acidic-functionalized ionic liquid as corrosion inhibitor for 304 stainless steel in aqueous sulfuric acid. *ACS Sustainable Chemistry & Engineering*, *4*(9), 5046-5052.

Madkour, L. H., Kaya, S., Guo, L., & Kaya, C. (2018). Quantum chemical calculations, molecular dynamic (MD) simulations and experimental studies of using some azo dyes as corrosion inhibitors for iron. Part 2: Bis–azo dye derivatives. *Journal of Molecular Structure*, *1163*, 397-417

Mobin, M., Zehra, S., &Aslam, R. (2016). L-Phenylalanine methyl ester hydrochloride as a green corrosion inhibitor for mild steel in hydrochloric acid solution and the effect of surfactant additive.*RSC advances*, *6*(7), 5890-5902.

Nkuna, A. A., Akpan, E. D., Obot, I. B., Verma, C., Ebenso, E. E., & Murulana, L. C. (2020). Impact of selected ionic liquids on corrosion protection of mild steel in acidic medium: Experimental and computational studies. *Journal of Molecular Liquids*, *314*, 113609.

Nkuzinna, O. C., Onukwuili, O. D., Nwanonenyi, S. C., Igboko, N., & Anusi, M. O. (2024). Ionic liquid as a potent and ecological benign corrosion constraint for aluminum in acidic medium. *Moroccan Journal of Chemistry*, *12*(1), 12-1.

Onukwuli, O. D., &Omotioma, M. (2019). Study of bitter leaves extract as inhibitive agent in HCl medium for the treatment of mild steel through prickling.*PortugaliaeElectrochimicaActa, 37* (2), 115-121.

Ortega Vega, M. R., Mattedi, S., Schroeder, R. M., & de Fraga Malfatti, C. (2021). 2-hydroxyethilammonium oleate protic ionic liquid as corrosion inhibitor for aluminum in neutral medium. *Materials and Corrosion*, *72*(3), 543-556.

Pancharatna, P. D., Lata, S., & Singh, G. (2019). Imidazolium based ionic liquid as an efficient and green corrosion constraint for mild steel at acidic pH levels. *Journal of Molecular Liquids*, *278*, 467-476.

Qiang, Y., Guo, L., Li, H., & Lan, X. (2021). Fabrication of environmentally friendly Losartan potassium film for corrosion inhibition of mild steel in HCl medium. *Chemical Engineering Journal*, *406*, 126863.

Qiang, Y., Zhang, S., Guo, L., Zheng, X., Xiang, B., & Chen, S. (2017). Experimental and theoretical studies of

four allylimidazolium-based ionic liquids as green inhibitors for copper corrosion in sulfuric acid.*Corrosion Science*, *119*, 68-78.

Quraishi, M. A., Chauhan, D. S., & Ansari, F. A. (2021). Development of environmentally benign corrosion inhibitors for organic acid environments for oil-gas industry. Journal of Molecular Liquids, 329, 115514.

Sasikumar, Y., Adekunle, A. S., Olasunkanmi, L. O., Bahadur, I., Baskar, R., Kabanda, M. M., ... & Ebenso, E. E. (2015). Experimental, quantum chemical and Monte Carlo simulation studies on the corrosion inhibition of some alkyl imidazolium ionic liquids containing tetrafluoroborate anion on mild steel in acidic medium. Journal of Molecular Liquids, 211, 105-118.

Shaban, S. M., Elbhrawy, M. F., Fouda, A. S., Rashwan, S. M., Ibrahim, H. E., & Elsharif, A. M. (2021). Corrosion inhibition and surface examination of carbon steel 1018 via N-(2-(2-hydroxyethoxy) ethyl)-N, N-dimethyloctan-1-aminium bromide in 1.0 M HCl. Journal of Molecular Structure, 1227, 129713.

Shetty, S. K., &Shetty, A. N. (2017). Eco-friendly benzimidazolium based ionic liquid as a corrosion inhibitor for aluminum alloy composite in acidic media. *Journal of Molecular Liquids*, *225*, 426-438.

Singh, A., Ansari, K. R., Banerjee, P., Murmu, M., Quraishi, M. A., & Lin, Y. (2021). Corrosion inhibition behaviour of piperidinium based ionic liquids on Q235 steel in hydrochloric acid solution: Experimental, density functional theory and molecular dynamics study. *Colloids and Surfaces A: Physicochemical and Engineering Aspects*, *623*, 126708.

Solomon, M. M., Umoren, S. A., Quraishi, M. A., Tripathy, D. B., & Abai, E. J. (2020). Effect of akyl chain length, flow, and temperature on the corrosion inhibition of carbon steel in a simulated acidizing environment by an imidazoline-based inhibitor. *Journal of Petroleum Science and Engineering*, *187*, 106801.

Su, H., Wang, L., Wu, Y., Zhang, Y., & Zhang, J. (2020). Insight into inhibition behaviour of novel ionic liquids for magnesium alloy in NaCl solution: experimental and theoretical investigation. Corrosion Science, 165, 108410.

Subasree, N., Selvi, J. A. (2020). Imidazolium based ionic liquid derivatives; synthesis and evaluation of inhibitory effect on mild steel corrosion in hydrochloric acid solution. Heliyon, 6(2), e03498. doi: 10.1016/j.heliyon.2020.e03498.

Tang, C., Stueber, M., Seifert, H. J., & Steinbrueck, M. (2017). Protective coatings on zirconium-based alloys as accident-tolerant fuel (ATF) claddings. *Corrosion Reviews*, *35*(3), 141-165.

Trabanelli, G. (2020). Corrosion inhibitors. In *Corrosion mechanisms* (pp. 119-163). CRC Press.

Umoren, S. A., Solomon, M. M., Ali, S. A., & Dafalla, H. D. (2019). Synthesis, characterization, and utilization of a diallylmethylamine-based cyclopolymer for corrosion mitigation in simulated acidizing environment. *Materials Science and Engineering: C*, *100*, 897-914

Umoren, S. A., Solomon, M. M., Ali, S. A., & Dafalla, H. D. (2019). Synthesis, characterization, and utilization of a diallylmethylamine-based cyclopolymer for corrosion mitigation in simulated acidizing environment. *Materials Science and Engineering: C*, *100*, 897-914.

Verma, C., Alrefaee, S. H., Quraishi, M. A., Ebenso, E. E., & Hussain, C. M. (2021). Recent developments in sustainable corrosion inhibition using ionic liquids: A review. *Journal of Molecular Liquids*, *321*, 114484.

Verma, C., Ebenso, E. E., & Quraishi, M. A. (2017). Ionic liquids as green and sustainable corrosion inhibitors for metals and alloys: an overview. *Journal of Molecular Liquids*, *233*, 403-414.

Verma, C., Ebenso, E. E., & Quraishi, M. A. (2018). Ionic liquids as green corrosion inhibitors for industrial metals and alloys. *Green Chemistry*.

Verma, C., Olasunkanmi, L. O., Bahadur, I., Lgaz, H., Quraishi, M. A., Haque, J., &Ebenso, E. E. (2019). Experimental, density functional theory and molecular dynamics supported adsorption behavior of environmental benign imidazolium based ionic liquids on mild steel surface in acidic medium. Journal of Molecular Liquids, 273, 1-15.

Wang, D., Li, Y., Chen, B., & Zhang, L. (2020).Novel surfactants as green corrosion inhibitors for mild steel in 15% HCl: Experimental and theoretical studies. *Chemical Engineering Journal*, *402*, 126219.

Xhanari, K., & Finšgar, M. (2019). Organic corrosion inhibitors for aluminum and its alloys in chloride and alkaline solutions: a review. Arabian Journal of Chemistry, 12(8), 4646-4663.

Yesudass, S., Olasunkanmi, L. O., Bahadur, I., Kabanda, M. M., Obot, I. B., & Ebenso, E. E. (2016). Experimental and theoretical studies on some selected ionic liquids with different cations/anions as corrosion inhibitors for mild steel in acidic medium. Journal of the Taiwan Institute of Chemical Engineers, 64, 252-268.

Zhang, S. Y., Zhuang, Q., Zhang, M., Wang, H., Gao, Z., Sun, J. K., & Yuan, J. (2020). Poly (ionic liquid) composites. *Chemical Society Reviews*, *49*(6), 1726-1755.

Zunita, M., & Kevin, Y. J. (2022). Ionic liquids as corrosion inhibitor: from research and development to commercialization. Results in Engineering, 15, 100562.